Effect of channel width on droplet generation inside T-junction microchannel

Santosh Kumar Jena, Tushar Srivastava, Supreet Singh Bahga, et al.

View Online   Export Citation   CrossMark

ARTICLES YOU MAY BE INTERESTED IN

Prediction of droplet sizes in a T-junction microchannel: Effect of dispersed phase inertial forces
Physics of Fluids 33, 032120 (2021); https://doi.org/10.1063/5.0039913

Non-Newtonian droplet breakup in a T-junction microdevice containing constriction induced asymmetric parallel branches
Physics of Fluids 35, 022004 (2023); https://doi.org/10.1063/5.0135186

Regulation of droplet size and flow regime by geometrical confinement in a microfluidic flow-focusing device
Physics of Fluids 35, 012010 (2023); https://doi.org/10.1063/5.0130834
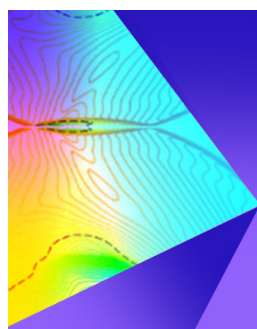
Physics of Fluids

Special Topic: Shock Waves

Submit Today!

AIP Publishing

Effect of channel width on droplet generation inside T-junction microchannel

View Online   Export Citation   CrossMark

Santosh Kumar Jena,[1] (iD) Tushar Srivastava,[1] (iD) Supreet Singh Bahga,[2] (iD) and Sasidhar Kondaraju[1,a)] (iD)

AFFILIATIONS

[1]School of Mechanical Sciences, Indian Institute of Technology Bhubaneswar, Argul, Khurda, Bhubaneswar, Odisha 752050, India
[2]Department of Mechanical Engineering, Indian Institute of Technology Delhi, Hauz Khas, New Delhi 110016, India

[a)]Author to whom correspondence should be addressed: sasidhar@iitbbs.ac.in. **URL:** https://www.iitbbs.ac.in/profile.php/sasidhar

ABSTRACT

In a T-junction microchannel, channel geometry plays a major role that affects the physics behind droplet generation. The effect of channel width on droplet size and frequency in a T-junction microchannel is investigated in the present study. The current work is an extension of our previous work, where a model was developed to predict the size of the droplets generated in a T-junction microchannel when both the continuous and dispersed phase channels have equal widths. In the present work, we extended the model to account for the varying width ratio between the dispersed and continuous phase channels. We performed in-house experiments by varying the channel width and viscosity ratios between the fluids to study the size of the droplets generated and to validate the proposed scaling law. We further investigated the effect of channel geometry on the frequency of droplet generation in the T-junction microchannels. The experimental results show that the droplet length increases with an increase in the width of the continuous phase channel. On the other hand, the droplet production frequency decreases with an increase in the width of the continuous phase channel. With variations in the width of the dispersed phase channel, similar behavior in droplet sizes and the frequency of droplet production is observed. The analysis of this study provides new insight into the effect of channel width on the droplet length and frequency. Overall, this research intends to provide a thorough understanding of the design of microchannels based on the geometry and manipulation of droplets with varying widths.

I. INTRODUCTION

Nowadays droplet-based technology provides a wide range of platforms for producing micro- and nanodroplet in a channel having a cross section in the order of a micrometer. Because of precise and controlled droplet generation, the faster reaction inside the microchannel, and interdisciplinary applications, it has attracted remarkable attention over the past 20 years. Apart from fundamental and technical aspects, droplet microfluidics has many broad areas of applications such as drug delivery,[1,2] biology,[3–5] clinical diagnostics,[6] materials science,[7] and emulsions in food[8] and textile industries. Droplet microfluidics serves as the foundation for cell encapsulation and digital polymerase chain reaction, which enables single cell analysis and quick diagnosis of a variety of diseases. Using this method, water in oil (W/O), oil in water (O/W), and gas–liquid droplet generation in microchannel having a particular size and pattern is possible. The advantages of droplet microfluidics include simple and resilient droplet generation, superior handling, production of monodisperse droplets, and precise droplet control. The produced droplets can be controlled independently with increased throughput, scalability, and substantial consistency.[9]

To date, microchannels having rectangular-, square-,[10] circular-,[11] and U-shaped[12] cross sections have been investigated. The rapid advancement of microfabrication technology permits droplet microfluidics for enhanced control over diverse fluid interface interactions and manipulation of discrete droplets within microchannels. To generate homogeneous droplets inside a microchannel, many microfluidic techniques such as co-flow,[13–15] T-junction,[16–19] and flow-focusing[20–22] have been put forward. Due to monodispersed droplet formation, simplicity in design, ease of manufacturing, and faster reactions inside a microchannel, T-junction is extensively used for droplet generations.[16–18,23–25] Recently, researchers have modified the T-junction with a contractive structure[26–28] and a step structure[29] and initiated a study into the physics underlying droplet dynamics. Both active[30,31] and passive techniques[32] were used for the generation of droplets. T-junction is a passive method of droplet generation, in which the monodispersed droplets with uniform spacing between the droplets are generated. The current work focuses on the T-junction having a rectangular cross section.

Thorsen *et al.*[16] first reported the formation of aqueous droplets in oil in a T-junction using pressure-controlled flow. They explained

the dynamics of droplet size generation in terms of tangential shear stresses and interfacial forces. Later, several studies[17,18,33–37] were carried out to understand the effect of different parameters. The factors responsible for the droplet formation within a T-junction are geometrical parameters such as channel width, flow properties such as the flow rate of the continuous and dispersed phases, pressures at the inlet of the channel, fluid properties such as viscosity,[38,39] interfacial tension, and wetting properties such as contact angle.[40] The effect of these properties can be formulated as the non-dimensional numbers, such as the capillary number of the continuous phase (Ca_c), the Weber number of the dispersed phase (We_d), the flow rate ratio between the dispersed phase fluid and the continuous phase fluid (ϕ), and the widths of the dispersed phase channel to the continuous phase channel (w_d/w_c).

Three important regimes, namely, the squeezing regime that occurs at low Ca_c, the dripping regime at moderate Ca_c, and the jetting regime at high Ca_c, were extensively investigated. Researchers found that the size of the droplets generated in squeezing and dripping regimes can be controlled and, thus, termed the regimes as stable. However, the jetting regime is accompanied by instabilities along the flow, which complicate the task of controlling droplet sizes.[41] Christopher et al.[42] investigated the effect of capillary number, flow rate ratio, channel geometry, and viscosity ratio for droplet breakup in the T-junction. They varied the dispersed phase channel width (w_d) while maintaining the constant depth (h) and the width of the continuous phase channel (w_c). The same group observed that the droplet volume is nearly constant for width ratio (w_d/w_c) less than one and increases linearly for ratios greater than one for different capillary numbers, and is highly responsive to width ratio for low Ca_c. Droplet generation rate using T-channel first proclaimed by Nisisako group.[18] Their group discovered that frequency increases linearly with an increase in continuous phase velocity. Later, Christopher and co-workers[42] showed that the droplet formation frequency increases with capillary number but is inversely related to droplet volume. They argued that the frequency increases linearly at low Ca, followed by a power-law behavior ($f \propto Ca^{4/3}$) at higher Ca. Wehking et al.[43] experimentally studied the effect of channel geometry on droplet generation and frequency by varying the aspect ratio (h/w_c) while maintaining h constant, where h is the channel height and w_c is the width of the continuous phase channel. They found that droplet volume decreases and production rate increases as the aspect ratio increases. Though many scaling laws were developed for the droplet size, appropriate physics is still lacking, when both the channel widths are varying. Recently, Jena et al.[37] developed an extensive model for predicting droplet length with uniform channel width for both the continuous and dispersed phase fluid. The developed model works very well for both the squeezing and dripping regimes. Along with the three major forces pressure force, shear force, and interfacial tension, the developed model includes the inertial force of the dispersed phase for droplet breakup and predicts the droplet size.

In the current work, we carried out experiments on T-junction microchannels having continuous phase channel widths (w_c) of 250, 280, 350, and 440 μm and dispersed phase channel widths (w_d) of 250, 360, and 460 μm. Fluid combinations having different viscosity ratios $\lambda = \mu_d/\mu_c$ were chosen. During the experiments, the capillary number of the continuous phase (Ca_c), and the flow rate ratios (ϕ) were varied. In continuation of our previous work,[37] we formulated an analytical

model for the droplet size. The novelty of the present work is that, at a wide range of w_c, and w_d, we can predict the droplet size in both squeezing and dripping regimes. In our previous work, we established a model that functions effectively when the widths of both channels are identical. However, the model does not study the effect of channel widths on the breakup of the droplets. Though the effect of flow properties was established in our prior work, the current model demonstrates its robustness by forecasting the droplet lengths for the varying geometrical properties. The merging of the curves, irrespective of flow rate and channel width for a particular fluid, shows its potential in manipulating droplets inside the microchannel. A constant slope of 0.4 is seen for various continuous-phase fluids, demonstrating that the model can predict the droplet size for varying flow properties and geometrical properties.

II. MODEL FOR THE DROPLET SIZE HAVING DIFFERENT CONTINUOUS PHASE CHANNEL WIDTH

Droplet generation in a microfluidic T-junction occurs due to the competition of different forces between the continuous phase fluid and the dispersed phase fluid flowing through the channel. Figure 1 depicts a three-dimensional view of the T-junction as well as channels with variable widths. w_c and w_d are the inlet channel widths, and h is the depth of the channel, where subscripts c and d stand for continuous and dispersed phases. Continuous phase fluid (oil) flows through the main channel, and the side channel is used for the transport of dispersed phase fluid (DIW). When the two liquids meet at the junction, an interface is created, which grows depending on the forces acting on it. After some time, necking takes place at the junction's interface, which continues to become narrow as the flow continues and droplet
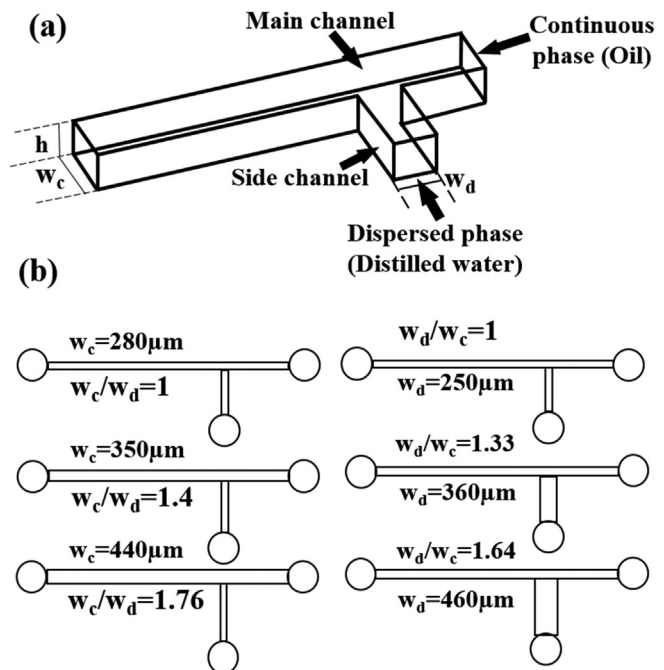

FIG. 1. (a) Three-dimensional view of microfluidic T-junction. (b) Configuration of different channel geometry used for conducting the experiment. For all channels, h is taken as 200 μm.

breakup takes place. The formation of droplets inside the microchannel is influenced by a number of factors, including the geometry of the channel, the flow rate, and the viscosity of the fluid, among others. The current investigation focuses on the analytical modeling of the droplet size by modifying our previous model. The model includes the effect of different continuous phase channel widths on droplet generation. The primary forces studied are the pressure difference at the upstream and downstream edges of the droplet (F_p), shear forces from the continuous phase (F_τ), force due to interfacial tension (F_σ), and the dispersed phase inertia force. The summary of the abbreviations is included in the nomenclature of the supplementary material.

Using Newton's second law of motion suggests that the rate of change of momentum of a control mass accounts for the net force acting on it. A schematic of the control mass of the droplet with other variables is shown in Fig. 2. Referring to our previous work,[37] when a detachment of droplet happened, we could write, $d(mu)/dt = \sum F_{external}$.

$$F_\tau + F_p - F_\sigma = m\frac{du}{dt} + u\frac{dm}{dt}, \quad (1)$$

where m and u are the mass and velocity of the control mass, respectively. The pressure force (F_P) and shear force (F_τ) act to deform the droplet, and the force due to interfacial tension (F_σ) resists the deformation of the droplet. When the gap between the droplet interface and the top wall of the channel (w_g) is very small as compared to w_c, the pressure force is estimated using lubrication analysis as $F_p = \Delta p w_c h \sim O(\mu Q_c w_c L/w_g^3)$. The shear force and force due to interfacial tension are estimated as $F_\tau = \tau w_c h \sim O(\mu Q_c L/w_g^2)$ and $F_\sigma \sim \sigma h$, respectively. Using these forces and expanding Q_c, the analytical model is developed for varying w_c and w_d. By considering the above three forces from Garstecki et al.,[17] the modified equation can be written as

$$\mu_c U_c L \left(\frac{w_c}{w_g^2}\right)h + \mu_c U_c L \left(\frac{w_c^2}{w_g^3}\right)h \sim \sigma h + \rho_d U_d w_d hu. \quad (2)$$

The length of the droplet L in Eq. (2) will be non-dimensionalized by using the length scale l_s which is taken as w_d for the channels with varying continuous phase channel width and as w_c when the dispersed phase channel width is varied. The velocity u in the last term of the Eq. (2) is scaled as the average of the continuous phase and the
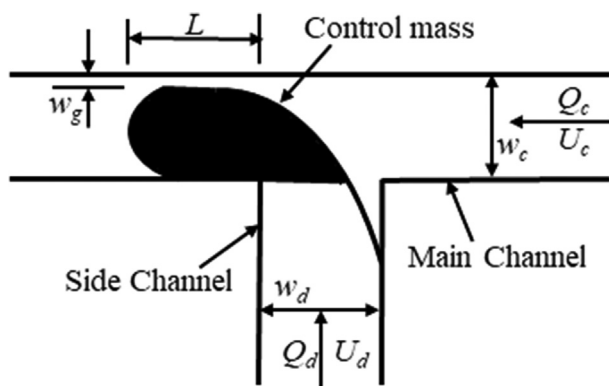
dispersed phase velocities (i.e., $u \sim (U_c + U_d)/2$. By applying the above-mentioned scaling to the equation and dividing throughout with σh, the equation can be rewritten as

$$Ca_c \frac{L}{l_s}\left(\frac{w_c l_s}{w_g^2}\right) + Ca_c \frac{L}{l_s}\left(\frac{w_c l_s}{w_g^3}\right) \sim 1 + We_d \left(\frac{\frac{w_d}{w_c} + \phi}{2\phi}\right). \quad (3)$$

Here, We_d is the dispersed phase Weber number, and Ca_c is the continuous phase capillary number. Equation (3) implies that the forces from the continuous phases that try to break up the dispersed phase thread are balanced by the dispersed phase inertial forces that prevent the thinning of the dispersed phase neck. Equation (3) can be represented as follows:

$$\frac{L}{l_s}Ca_c f\left(\frac{w_c l_s}{w_g}\right) \sim 1 + We_d \left(\frac{\frac{w_d}{w_c} + \phi}{2\phi}\right). \quad (4)$$

The scaling model presented in the manuscript considers all the important forces responsible for droplet breakup inside a T-junction microchannel. The proposed model works well for both the continuous phase and dispersed phase channel widths for predicting droplet length which is not addressed until now.

III. EXPERIMENTAL PROCEDURE

A wide range of experiments was conducted for varying continuous phase channel width by using silicone oil and hexadecane oil as continuous phase fluids (Sigma Aldrich). Distilled water (DIW) was taken as the dispersed phase in all cases. The fluids are Newtonian in nature. The continuous phase fluids were selected to show the effect of viscosity variations. The physical properties of the fluids and flow parameters that varied in the experiments are given in Table I. The viscosity was measured using a rheometer (cone and plate type, Anton Paar) and an Oswald viscometer (U-tube type). The pendant drop method[44] was used for interfacial tension measurement with an accuracy of 98%. Computer numerical control (CNC) micro milling (The Cool Tool®) and thermal bonding techniques were employed to manufacture the different microchannels. The thermal bonding technique is used to seal the two sheets of polymethyl methacrylate (PMMA) for 45 min, and then the channel is allowed to cool for 30–45 min. A 200 μm diameter end mill tool is used for preparing the microchannel on a (PMMA) sheet of dimension $50 \times 30 \times 5 \, mm^3$. Different continuous phase channel widths having dimensions of 250, 280, 350, and 440 μm were fabricated. The channels with varying w_c have a uniform dispersed phase width of 250 μm. Also, channels with varying dispersed phase widths ($w_d = 250$, 360, and 460 μm) are

FIG. 2. A schematic of a typical T-junction.

TABLE I. The physical properties of two continuous phase fluids are specified here. For dispersed phase fluid, distilled water (DIW) is taken for conducting experiments. The dynamic viscosity and density of DIW are $\mu_d = 0.99 \, mPa \, s$, and $\rho_d = 1000 \, kg/m^3$, respectively.

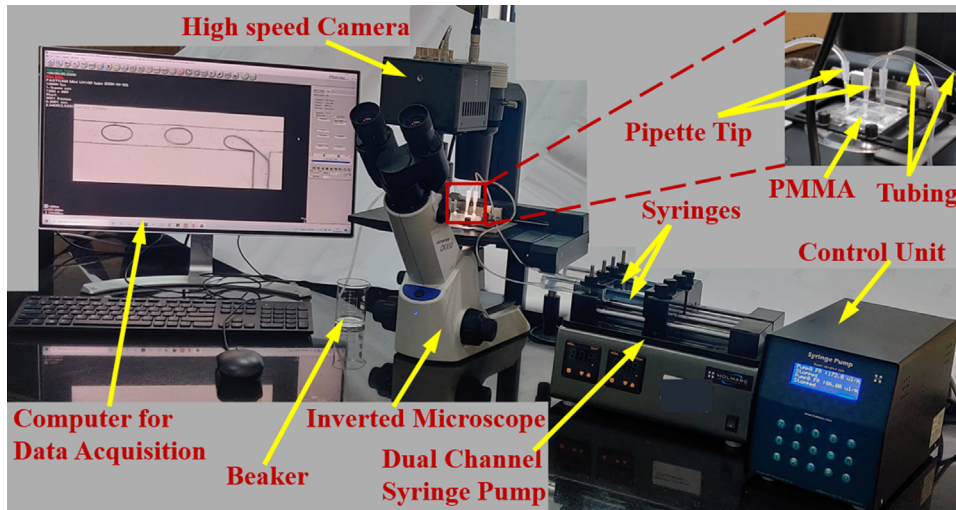| Continuous phase	ρ (kg/m³)	ϕ	λ	σ (mN/m)
Hexadecane	773	0.25, 0.5, and 1.0	0.4167	37.68
Silicone oil	960	0.25, 0.5, and 1.0	0.0146	48.15

FIG. 3. The in-house experimental set up developed for generating droplets inside microfluidic T-junction is shown here. The channel has two inlets and one outlet. The cross section of the channel is rectangular.

prepared. All the channels have a uniform depth of 200 μm. Initially, the channel was hydrophilic in nature and converted to hydrophobic with the chemical treatment of aquapel solution (Pittsburgh Glass Works LLC, USA). To inject the fluids through the microfluidic T-junction, a dual-channel syringe pump (Holmarc Inc.) was used. First, priming is carried out by flowing continuous phase liquid through the main channel, and then dispersed phase fluid is injected from the side channel to generate droplets. For visualizing the droplet production process, an inverted microscope (Olympus, Japan) was used. A high-speed camera (Photron FASTCAM mini UX) was used to record the experimental occurrence of droplet generation at 10 000 frames per second with a resolution of 1280 × 480 pixels. Then, post-processing of the video was accomplished frame by frame to quantify the parameters. The image processing and data analysis of the experimental results were carried out using the Photron FASATCAM viewer and ImageJ software. The high-speed camera's built-in Photron FASTCAM Viewer software is utilized for measuring the length of the droplet during the post-processing of the images. We calibrate the software to our specifications prior to measuring the image. Our measurements involve an objective lens with a 4× magnification and images recorded at a rate of 10 000 frames per second. We used a glass slide calibrator to obtain the relationship between the pixels and the physical lengths in micrometer. In our case, it is 2.54 μm/pixel. All the experiments were performed at room temperature (about 25 °C). The observations were taken once the device reached a steady state after setting the flow rates for each phase. Each experiment was conducted three times, and L/w_d is taken as the average of the individual experimental runs. The assembled in-house experimental setup is shown in Fig. 3.

IV. RESULTS AND DISCUSSION

Water droplets in oil were generated by injecting oil (continuous phase fluid) in the main channel and DIW (dispersed phase fluid) in the side channel. To acknowledge the effect of different w_c on droplet generation, the experimental results are plotted in Fig. 4. Three distinct regimes, i.e., squeezing, dripping, and jetting, are found during the droplet formations in all three continuous phase channel widths.

However, the transition point from squeezing to dripping and dripping to jetting decreases as w_c increases.

The length of the droplet decreases with an increase in the continuous phase capillary number, which follows a similar trend for all the three continuous phase channel widths as shown in Fig. 4. It is also observed from the experiments that with an increase in w_c, the droplet length increases for both fluid combinations. The possible reason could be that as w_c increases, the flow rate of continuous phase fluid increases, which imposes a larger inertia force on the protruding interface. For the same Ca_c, the increased w_c drags the interface to a larger length before droplet breakup occurs. It was previously found that when Ca_c increases, the droplet length decreases. Hence, the gap
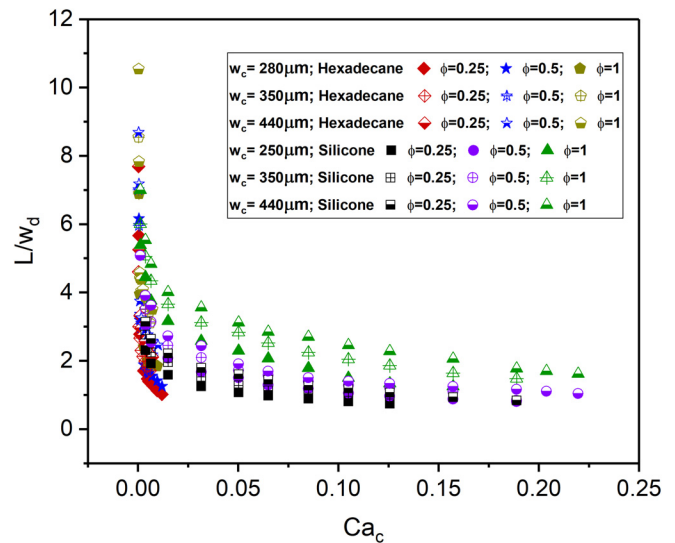

FIG. 4. L/w_d is plotted against the Ca_c for w_c = 250, 280, 350, and 440 μm for hexadecane and silicone oil as continuous phase fluid for different ϕ. The non-dimensional droplet length L/w_d decreases with an increasing capillary number Ca_c and increases with an increase in w_c and ϕ.

between the interface of the droplet and the main channel wall (w_g) increases. For varying w_c, it was noticed from our experimental findings that w_g increases with an increase in w_c, which is in accordance with the model shown in Eq. (4).

For a constant Ca_c, the results are shown in Fig. S1 in the supplementary material, along with the corresponding experimental images in Fig. S2. Moreover, it can be observed from our model that the ratio of w_c/w_g inversely affects Ca_c. Our in-house experimental results show the same phenomena for different w_c and fluid combinations. In another set of experiments, we vary dispersed phase channel width (w_d). When w_d varies from 250 to 460 μm, the droplet length increases. When w_d increases, the velocity of the dispersed phase decreases. As a result, the movement of the interface becomes shorter, which will slow down the penetration. Before breaking up, the interface expands to a greater length, and the droplet's length continues to grow. Experiments are conducted by using silicone oil as a continuous phase fluid for flow rate ratios of 0.5 and 1. The non-dimensional droplet length is taken as L/w_c and the results are depicted in Fig. 5. The experimental results presented in the manuscript are conducted three times for each data point and the average of the data are taken. The maximum uncertainty in the measurement of length is ± 0.05 and for frequency, it is ± 0.06.

Equation (4) suggests that w_g is directly proportional to both w_c and Ca_c. From Fig. S1, it is observed that the slope of w_g/w_c is nearly constant at low Ca_c, which increases with an increase in Ca_c. At a constant Ca_c, as w_c increases, the change in slope is greater, which occurred due to the increase in the flow rate of the continuous phase. When w_c is larger, the shear force tends to dominate, which causes the interface to become narrower before it blocks the main channel. This results in an increase in w_g for a given Ca_c. Based on the findings of the study, it can be concluded that w_g is more responsive toward w_c at
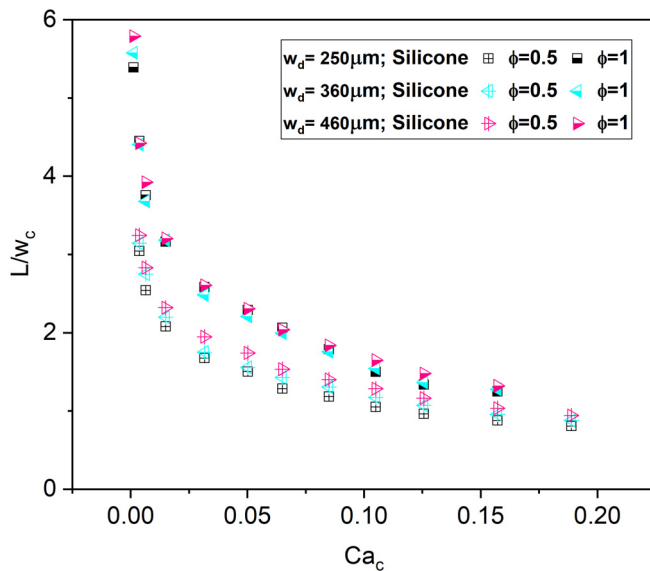
FIG. 5. L/w_c is plotted against the Ca_c for $w_d = 250$, 360, and 460 μm for silicone oil as continuous phase fluid for different ϕ. The non-dimensional droplet length L/w_c decreases with an increasing capillary number Ca_c and increases with an increase in w_d and ϕ.

Constant We$_d$

(a) We$_d$=1.59 x 10^{-2} , w_g=137μm

(b) We$_d$=1.39 x 10^{-2} , w_g=160μm

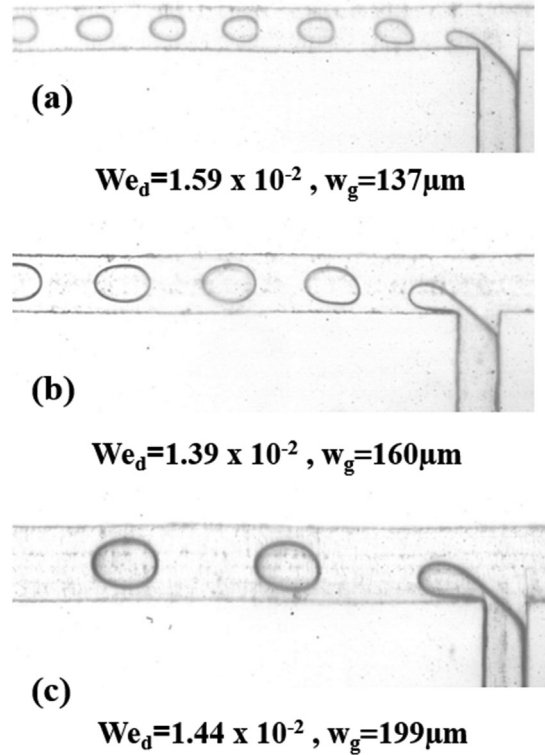(c) We$_d$=1.44 x 10^{-2} , w_g=199μm

FIG. 6. Experimental images illustrating droplet length and w_g for w_c: (a) 250, (b) 350, and (c) 440 μm for a constant We_d. It was noticed that w_g increases from 137 to 199 μm as w_c increases from 250 to 440 μm. The results shown here are for silicone oil as a continuous phase fluid with a flow rate ratio $\phi = 0.5$.

higher Ca_c. Our experimental findings further imply that, for a fixed We_d, both the droplet length and w_g increase with an increase in continuous phase channel widths (Fig. 6). At constant We_d, the inertia force of the dispersed phase, which opposes the neck from becoming narrow, is constant. However, due to an increase in w_c, the pressure exerted by the continuous phase liquid on the dispersed phase fluid increases. Due to this, the dispersed phase liquid will take a longer time to build up sufficient pressure to penetrate the massive volume of the main channel. Our experimental findings demonstrate that for a fixed Ca_c, the time between penetration of interface till necking (t_{PN}) increases. As w_c increases, the increase in t_{PN} delays the interface to move along the flow. As a consequence of this, the interface is pulled to a greater length prior to the occurrence of droplet breakup, which contributes to an increase in droplet length. For a particular Ca_c, the t_{PN} for different w_c is shown in Fig. 7. When there is an increase in w_d, the dispersed phase velocity decreases, which results in an increase in t_{PN}. Because of this, the length of the droplet before it disintegrates is increased.

In our previous work, scaling was accomplished by taking results for a constant w_c. Considering our former model as a reference, we plot the results for different w_c by taking L/w_c as non-dimensional
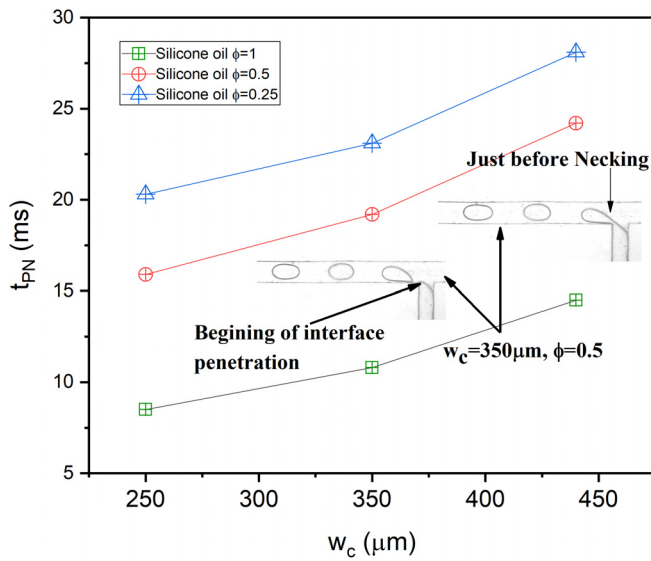
FIG. 7. Experimental images showing t_{PN} for $w_c = 250$, 350, and 440 μm for a constant Ca_c. It was observed that t_{PN} increases as w_c increases from 250 to 440 μm. The results are for silicone oil taken as a continuous phase liquid. All the results plotted here are for $Ca_c = 5.02 \times 10^{-2}$.

droplet length. For different w_c, the results are aligned in a parallel fashion to each other, as shown in Fig. 8. However, by altering the model by taking L/w_d as the dimensionless droplet length, we were able to see a single merged curve for a specific viscosity ratio.

From Eq. (4), it can be observed that for varying w_c, the non-dimensional droplet length L/w_d along with Ca_c depend on both We_d and w_c. We_d can be explained in terms of the inertia force of the dispersed phase, which counters the squeezing of the neck at the junction of the microchannel. Therefore, in Fig. 9, the plot displays $L/w_d \times Ca_c$
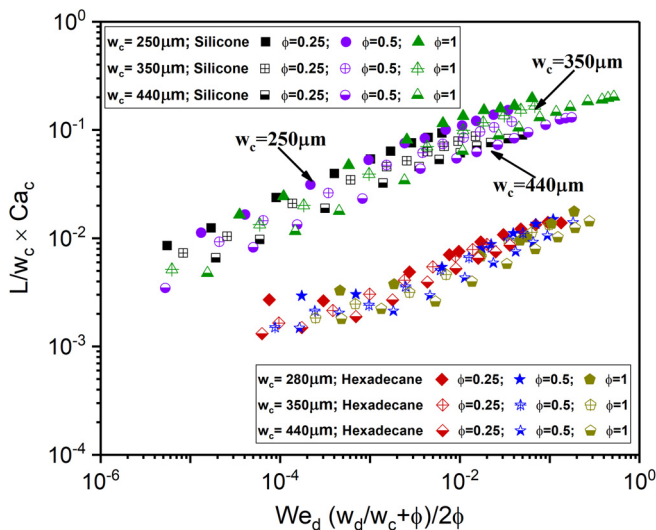

FIG. 8. $L/w_c \times Ca_c$ is plotted against the $We_d(\frac{\frac{w_d}{w_c}+\phi}{2\phi})$ on a log–log scale for different w_c, λ, and ϕ. The slope of the y-axis with respect to the x-axis is found to be 0.4.
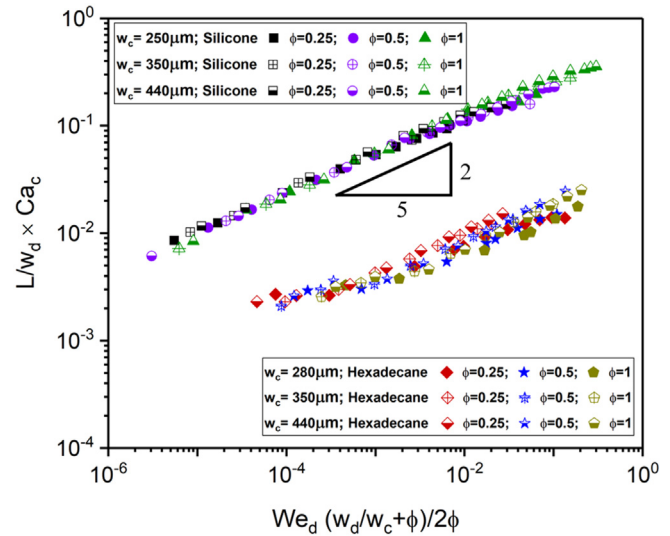

FIG. 9. $L/w_d \times Ca_c$ is plotted against the $We_d(\frac{\frac{w_d}{w_c}+\phi}{2\phi})$ on a log–log scale for different w_c, λ, and ϕ. The slope of the y-axis relative to the x-axis is found to be 0.4. For three different w_c, it is observed that the experimental results coalesce into a single curve for a particular fluid combination.

on vertical axis, whereas We_d $[(w_d/w_c) + \phi]/2\phi$ is displayed on the horizontal axis. As w_c increases, the shear force becomes more dominant over interfacial tension. The continuous phase exerts a significant amount of shear force that tries to squeeze the neck of the interface and drag it to move parallel with the flow. At the same time, the effect of the inertia force of the dispersed phase plays an important role in droplet breakup. The dispersed phase inertia force offers resistance in terms of dynamic pressure to the squeezing of the neck.[37] As the value of w_c increases from 250 to 440 μm, the droplet length increases due to the combined effects of w_c and the inertial force that results from the dispersed phase. We have performed statistical analysis for three aspect ratios (h/w_c) with a confidence level of 95%. The aspect ratios are 0.8 ($w_c = 250 \mu m$), 0.571($w_c = 350 \mu m$), and 0.454($w_c = 440 \mu m$) when silicone oil is utilized as the continuous phase. The aspect ratios for hexadecane oil as a continuous phase are 0.714 ($w_c = 280 \mu m$), 0.571($w_c = 350 \mu m$), and 0.454($w_c = 350 \mu m$). For all cases, the depth of the channel is maintained as 200 μm. With a confidence level of 95%, the droplet length can be predicted for different aspect ratio microchannels for silicone oil ($Ca_c = 0.0012$–0.22) and hexadecane ($Ca_c = 0.00015$–0.02), as indicated in the Figs. S4 and S5 in the supplementary material.

Additionally, we carried out studies by altering w_d taking silicone oil as the continuous phase. When w_d varies by plotting $L/w_d \times Ca_c$ against We_d $[(w_d/w_c) + \phi]/2\phi$, the results lay parallel to each other as shown in Fig. 10. The results are quite similar when w_c varies. By observing the results from varying w_c, for different w_d, we change the non-dimensional droplet length to L/w_c as w_c is constant. Then, $L/w_c \times Ca_c$ for different w_d is mapped against We_d $[(w_d/w_c) + \phi]/2\phi$. It is found that the curves merge to a single curve for different w_d. The results are shown in Fig. 11. From the plot, it can be observed that $L/w_c \times Ca_c$ increases with an increase in We_d $[(w_d/w_c) + \phi]/2\phi$ up to a certain point, beyond which there is a change in the slope. This shift
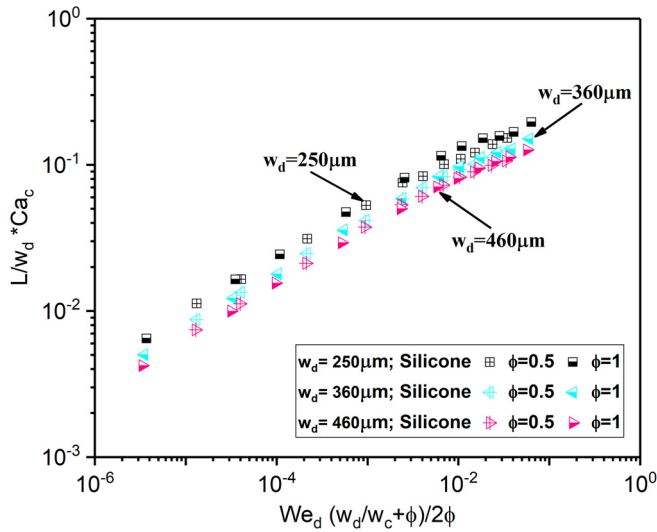
FIG. 10. $L/w_d \times Ca_c$ is plotted against the $We_d\left(\frac{\frac{w_d}{w_c}+\phi}{2\phi}\right)$ on a log–log scale for different w_c, λ, and ϕ. The slope of y-axis with respect to x-axis is found to be 0.4.

in slope suggests a transition from dripping to the jetting regime. For a specific viscosity ratio, it can be noticed from Fig. 11 that all the data collapse to a single curve, irrespective of dispersed phase channel widths and flow rate ratios. The above discussion leads us to the conclusion that channel width has a profound effect on droplet formation. It is possible to obtain a single merged curve for a given viscosity ratio when both the channel widths are varied while keeping other variables constant. From the model, we can predict the droplet size with respect to Ca_c by knowing the flow rate ratio (ϕ) and Weber number of the dispersed phase (We_d). Regardless of the flow rate ratios for a
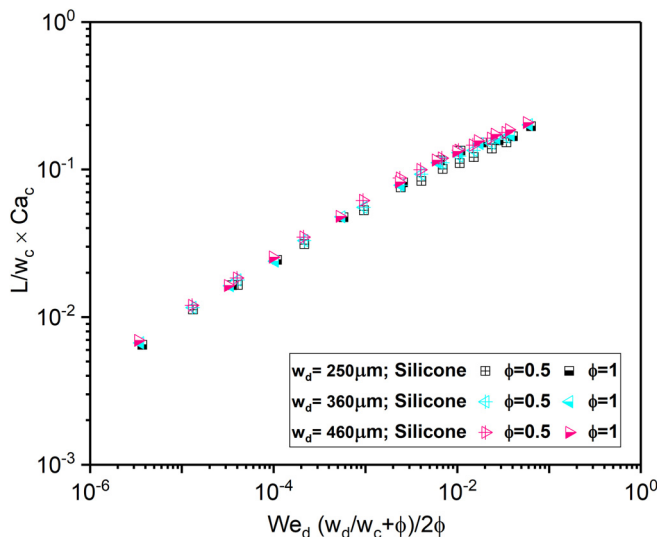
particular continuous phase fluid, the data are merged into a single curve, as depicted in Figs. 9 and 11. A constant slope of 0.4 is seen for various continuous-phase fluids, demonstrating that the model can predict the droplet size when both channel widths vary.

In addition to the droplet size, droplet production frequency is another important parameter that is addressed here. In the current work, the frequency of droplet generation is also analyzed. The frequency of droplet production depends upon the flow rate ratio, capillary number of the continuous phase, channel dimensions, and Weber number of the dispersed phase. Droplet production rates are calculated for three different continuous phase channel widths for varying flow rate ratios and fluid combinations. Based on the experimental footage, an estimate of the droplet formation rate per unit interval of time was developed. It is observed that the frequency increases with an increase in flow rate ratio but decreases with continuous phase channel width. In the research that has been provided, the flow rate ratio is altered by changing the flow rate of the dispersed phase while maintaining the constant flow rate of the continuous phase. As the flow rate ratio increases, the time it takes for the dispersed phase fluid to penetrate decreases. The shear force from the continuous phase breaks the interface quickly, which results in a faster formation rate. However, for a particular capillary number, with an increase in w_c, it offers higher resistance to penetration, which decreases the frequency generation rate. The results for frequency of droplet generation (f) concerning the capillary number of the continuous phase are plotted in Fig. 12 for different continuous phase channel widths. It is also observed that frequency increases slowly at low Ca_c but rapidly at higher Ca_c.

It is also noticed that for a fixed Ca_c, the production rate decreases with an increase in continuous phase channel width (w_c). The findings for different Ca_c are plotted and shown in Fig. S3. A similar behavior in the frequency of droplet generation is observed for the varying dispersed phase channel widths (w_d). The length of the droplet is observed to increase with an increase in the dispersed phase channel
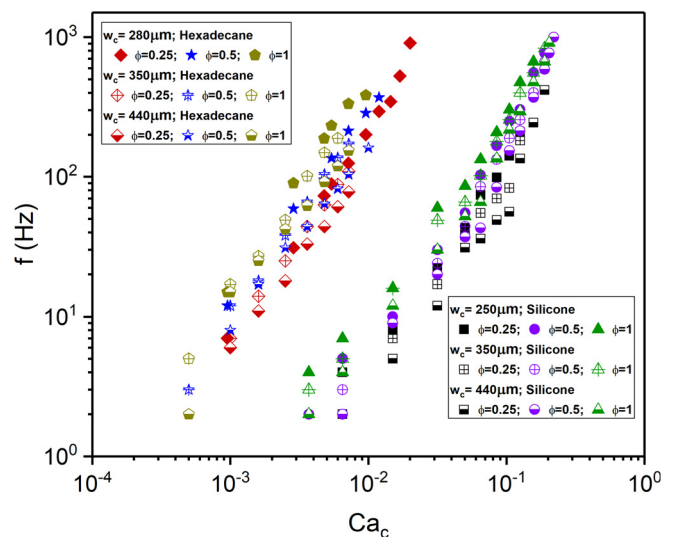

FIG. 11. $L/w_c \times Ca_c$ is plotted against the $We_d\left(\frac{\frac{w_d}{w_c}+\phi}{2\phi}\right)$ on a log–log scale for different w_c, λ, and ϕ. It is observed that the experimental results merge to a single curve for a silicone oil as continuous phase for three different w_d.

FIG. 12. The frequency of droplet generation (f) is mapped against the Ca_c for different w_c, λ, and ϕ. The experiments use hexadecane and silicone oil as continuous phase fluids.
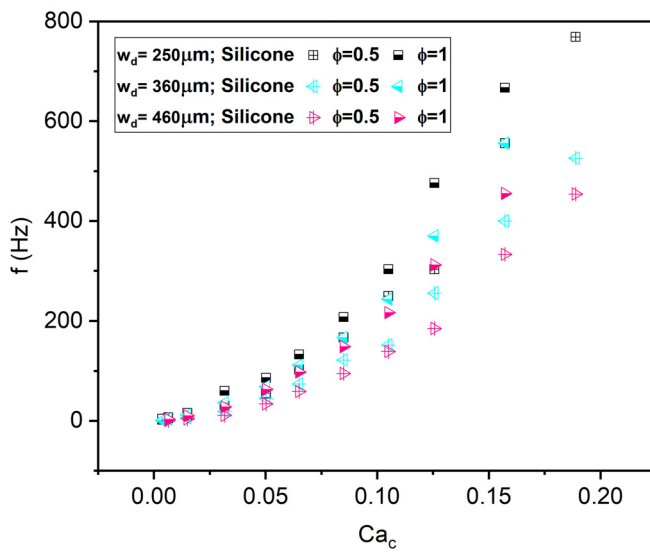
FIG. 13. The frequency of droplet formation (*f*) is plotted against the Ca_c for various w_d, λ, and ϕ values.

width and the frequency of the droplet generation is observed to decrease. Experiments are conducted for silicone oil as continuous phase fluid and the results for different w_d are shown in Fig. 13.

A scaling model has been developed in the present study which can quantify the effects of geometrical variations and flow properties. The model developed in this study has been validated for the channels with dimensions greater than or equal to 250 μm. However, for the microchannels with length scales of order 10 to 500 μm, the dominant forces acting on the droplet's interface are the same. Hence, it can be considered that the model presented in this study is applicable for microchannels of length scales in $O(20\,\mu m)$. Various researchers[17,38,42,45] conducted their studies using microchannels with dimensions ranging from 20 to 100 μm. They had used the same forces outlined in the current work for the analysis and development of the model. However, a comprehensive experimental study will be necessary to validate the present model for droplet generation inside the microchannels of $O(20\,\mu m)$.

V. CONCLUSIONS

In the present study, the investigation comprises a parametric analysis of the droplet size and frequency of droplet production for varying channel widths w_c and w_d. Though previous studies considered various channel parameters for predicting the droplet size, the physics behind the dynamics remained unclear. A theoretical analysis was carried out by taking into account Newtonian fluids without adding surfactants to either phase of the investigation. The model predicts the droplet size very well in both squeezing and dripping regimes for distinct w_c and w_d. The proposed mathematical model is validated with a large set of in-house experimental results that are consistent for different channel widths. In cases of varying w_c, the results lie parallel to each other when we take L/w_c as non-dimensional droplet length. However, the results collapse to a single curve when L/w_d is taken as non-dimensional droplet length. Reverse phenomena occurred when we vary dispersed channel width (w_d). However, the conducted

experiments are for channels having rectangular cross section only. The variation of frequency is presented in the current work at a wide range for varying w_c, ϕ, and λ. Also, the effect of different w_c on w_g, and t_{PN} are investigated thoroughly. The results show that both w_g and t_{PN} increase with an increment in w_c from 250 to 440 μm. The significance of the scaling model is that it assists in the geometry-based design of microchannels. Our experimental evidence proves its applicability for the manipulation of droplets within a T-junction for varying channel widths. While the current model is valid for various flow rate ratios, channel width ratios, and viscosity ratios, it has not been verified for shallow channels.

SUPPLEMENTARY MATERIAL

See the supplementary material for: The abbreviations of each variable are given in the nomenclature. Figure S1 shows the plot of w_g for w_c= 250, 350, and 440 μm, respectively. Corresponding experimental images are shown in Fig. S2. Figure S3 shows the plot for the frequency with respect to w_c for different Ca_c. Figures S4 and S5 depict the relationship between non-dimensional droplet length (L/w_d) and aspect ratio (h/w_c) for silicone and hexadecane oil as continuous phases, respectively.

AUTHOR DECLARATIONS
Conflict of Interest

The authors have no conflicts to disclose.

Author Contributions

Santosh Kumar Jena: Conceptualization (lead); Investigation (lead); Methodology (lead). **Tushar Srivastava:** Investigation (supporting); Methodology (supporting). **Supreet Singh Bahga:** Funding acquisition (equal); Methodology (equal). **Sasidhar Kondaraju:** Funding acquisition (equal); Investigation (equal); Methodology (equal); Supervision (equal); Writing – review & editing (equal).

DATA AVAILABILITY

The data that support the findings of this study are available from the corresponding author upon reasonable request.

REFERENCES

[1]L. Shang, Y. Cheng, and Y. Zhao, "Emerging droplet microfluidics," Chem. Rev. **117**, 7964–8040 (2017).
[2]S. Sohrabi, M. K. Moraveji *et al.*, "Droplet microfluidics: Fundamentals and its advanced applications," RSC Adv. **10**, 27560–27574 (2020).
[3]J. Chen, D. Chen, Y. Xie, T. Yuan, and X. Chen, "Progress of microfluidics for biology and medicine," Nano-Micro Lett. **5**, 66–80 (2013).

[4] S. Mashaghi, A. Abbaspourrad, D. A. Weitz, and A. M. van Oijen, "Droplet microfluidics: A tool for biology, chemistry and nanotechnology," TrAC, Trends Anal. Chem. **82**, 118–125 (2016).

[5] T. S. Kaminski, O. Scheler, and P. Garstecki, "Droplet microfluidics for microbiology: Techniques, applications and challenges," Lab Chip **16**, 2168–2187 (2016).

[6] K. V. Kaler and R. Prakash, "Droplet microfluidics for chip-based diagnostics," Sensors **14**, 23283–23306 (2014).

[7] J. I. Park, A. Saffari, S. Kumar, A. Günther, and E. Kumacheva, "Microfluidic synthesis of polymer and inorganic particulate materials," Annu. Rev. Mater. Res. **40**, 415–443 (2010).

[8] K. Muijlwijk, C. Berton-Carabin, and K. Schroën, "Cross-flow microfluidic emulsification from a food perspective," Trends Food Sci. Technol. **49**, 51–63 (2016).

[9] G. F. Christopher and S. L. Anna, "Microfluidic methods for generating continuous droplet streams," J. Phys. D **40**, R319 (2007b).

[10] H. Becker and L. E. Locascio, "Polymer microfluidic devices," Talanta **56**, 267–287 (2002).

[11] M. Abdelgawad, C. Wu, W.-Y. Chien, W. R. Geddie, M. A. Jewett, and Y. Sun, "A fast and simple method to fabricate circular microchannels in polydimethylsiloxane (PDMS)," Lab Chip **11**, 545–551 (2011).

[12] S. Prakash, B. Acherjee, A. S. Kuar, and S. Mitra, "An experimental investigation on Nd:Yag laser microchaneling on polymethyl methacrylate submerged in water," Proc. Inst. Mech. Eng., Part B **227**, 508–519 (2013).

[13] Y. Chen, L. Wu, and C. Zhang, "Emulsion droplet formation in coflowing liquid streams," Phys. Rev. E **87**, 013002 (2013).

[14] P. Zhu, X. Tang, and L. Wang, "Droplet generation in co-flow microfluidic channels with vibration," Microfluid. Nanofluid. **20**, 47 (2016).

[15] T. Nisisako, T. Torii, T. Takahashi, and Y. Takizawa, "Synthesis of monodisperse bicolored Janus particles with electrical anisotropy using a microfluidic co-flow system," Adv. Mater. **18**, 1152–1156 (2006).

[16] T. Thorsen, R. W. Roberts, F. H. Arnold, and S. R. Quake, "Dynamic pattern formation in a vesicle-generating microfluidic device," Phys. Rev. Lett. **86**, 4163 (2001).

[17] P. Garstecki, M. J. Fuerstman, H. A. Stone, and G. M. Whitesides, "Formation of droplets and bubbles in a microfluidic T-junction—Scaling and mechanism of break-up," Lab Chip **6**, 437–446 (2006).

[18] T. Nisisako, T. Torii, and T. Higuchi, "Droplet formation in a microchannel network," Lab Chip **2**, 24–26 (2002).

[19] S. Van der Graaf, T. Nisisako, C. Schroën, R. Van Der Sman, and R. Boom, "Lattice Boltzmann simulations of droplet formation in a T-shaped microchannel," Langmuir **22**, 4144–4152 (2006).

[20] T. Cubaud and T. G. Mason, "Capillary threads and viscous droplets in square microchannels," Phys. Fluids **20**, 053302 (2008).

[21] S. Wu, J. Chen, X. Liu, and F. Yao, "Experimental study of droplet formation in the cross-junction," J. Dispersion Sci. Technol. **42**, 1233 (2021).

[22] X. Chen, T. Glawdel, N. Cui, and C. L. Ren, "Model of droplet generation in flow focusing generators operating in the squeezing regime," Microfluid. Nanofluid. **18**, 1341–1353 (2015).

[23] S. Van Loo, S. Stoukatch, M. Kraft, and T. Gilet, "Droplet formation by squeezing in a microfluidic cross-junction," Microfluid. Nanofluid. **20**, 146 (2016).

[24] J. Husny and J. J. Cooper-White, "The effect of elasticity on drop creation in T-shaped microchannels," J. Non-Newtonian Fluid Mech. **137**, 121–136 (2006).

[25] S. Mehraji and M. Saadatmand, "Flow regime mapping for a two-phase system of aqueous alginate and water droplets in T-junction geometry," Phys. Fluids **33**, 072009 (2021).

[26] Z. Liu, J. Zhao, Y. Pang, and X. Wang, "Generation of droplets in the T-junction with a constriction microchannel," Microfluid. Nanofluid. **22**, 124 (2018).

[27] X. Li, L. He, Y. He, H. Gu, and M. Liu, "Numerical study of droplet formation in the ordinary and modified T-junctions," Phys. Fluids **31**, 082101 (2019).

[28] Y. Pang, Q. Yang, X. Wang, and Z. Liu, "Dripping and jetting generation mode in T-junction microchannels with contractive structures," Phys. Fluids **34**, 092001 (2022).

[29] S. Da Ling, J. Zhang, Z. Chen, W. Ma, Y. Du, and J. Xu, "Generation of monodisperse micro-droplets within the stable narrowing jetting regime: Effects of viscosity and interfacial tension," Microfluid. Nanofluid. **26**, 53 (2022).

[30] Z. Z. Chong, S. H. Tan, A. M. Gañán-Calvo, S. B. Tor, N. H. Loh, and N.-T. Nguyen, "Active droplet generation in microfluidics," Lab Chip **16**, 35–58 (2016).

[31] R. Singh, S. Bahga, and A. Gupta, "Electrohydrodynamic droplet formation in a T-junction microfluidic device," J. Fluid Mech. **905**, A29 (2020).

[32] P. Zhu and L. Wang, "Passive and active droplet generation with microfluidics: A review," Lab Chip **17**, 34–75 (2017).

[33] H. A. Stone, A. D. Stroock, and A. Ajdari, "Engineering flows in small devices: Microfluidics toward a lab-on-a-chip," Annu. Rev. Fluid Mech. **36**, 381–411 (2004).

[34] J. H. Xu, S. Li, J. Tan, and G. Luo, "Correlations of droplet formation in T-junction microfluidic devices: From squeezing to dripping," Microfluid. Nanofluid. **5**, 711–717 (2008).

[35] T. Glawdel, C. Elbuken, and C. L. Ren, "Droplet formation in microfluidic T-junction generators operating in the transitional regime. I. Experimental observations," Phys. Rev. E **85**, 016322 (2012).

[36] J. D. Tice, A. D. Lyon, and R. F. Ismagilov, "Effects of viscosity on droplet formation and mixing in microfluidic channels," Anal. Chim. Acta **507**, 73–77 (2004).

[37] S. K. Jena, S. S. Bahga, and S. Kondaraju, "Prediction of droplet sizes in a T-junction microchannel: Effect of dispersed phase inertial forces," Phys. Fluids **33**, 032120 (2021).

[38] J. Yao, F. Lin, H. S. Kim, and J. Park, "The effect of oil viscosity on droplet generation rate and droplet size in a T-junction microfluidic droplet generator," Micromachines **10**, 808 (2019).

[39] M. Nekouei and S. A. Vanapalli, "Volume-of-fluid simulations in microfluidic T-junction devices: Influence of viscosity ratio on droplet size," Phys. Fluids **29**, 032007 (2017).

[40] M. P. Boruah, A. Sarker, P. R. Randive, S. Pati, and S. Chakraborty, "Wettability-mediated dynamics of two-phase flow in microfluidic T-junction," Phys. Fluids **30**, 122106 (2018).

[41] M. De Menech, P. Garstecki, F. Jousse, and H. A. Stone, "Transition from squeezing to dripping in a microfluidic T-shaped junction," J. Fluid Mech. **595**, 141–161 (2008).

[42] G. F. Christopher, N. N. Noharuddin, J. A. Taylor, and S. L. Anna, "Experimental observations of the squeezing-to-dripping transition in T-shaped microfluidic junctions," Phys. Rev. E **78**, 036317 (2008).

[43] J. D. Wehking, M. Gabany, L. Chew, and R. Kumar, "Effects of viscosity, interfacial tension, and flow geometry on droplet formation in a microfluidic T-junction," Microfluid. Nanofluid. **16**, 441–453 (2014).

[44] N.-A. Goy, Z. Denis, M. Lavaud, A. Grolleau, N. Dufour, A. Deblais, and U. Delabre, "Surface tension measurements with a smartphone," Phys. Teach. **55**, 498–499 (2017).

[45] T. Glawdel, C. Elbuken, and C. L. Ren, "Droplet formation in microfluidic T-junction generators operating in the transitional regime. II. Modeling," Phys. Rev. E **85**, 016323 (2012).